Transitional properties of supersolitons in a two electron temperature warm multi-ion plasma

Steffy S. Varghese and S. S. Ghosh

Citation: Physics of Plasmas **23**, 082304 (2016); doi: 10.1063/1.4959851
View online: http://dx.doi.org/10.1063/1.4959851
View Table of Contents: http://scitation.aip.org/content/aip/journal/pop/23/8?ver=pdfcov
Published by the AIP Publishing

Transitional properties of supersolitons in a two electron temperature warm multi-ion plasma

Steffy S. Varghese[a] and S. S. Ghosh[b]
Indian Institute of Geomagnetism, New Panvel(W), Navi Mumbai, India

(Received 3 June 2016; accepted 10 July 2016; published online 4 August 2016)

The existence domain of an ion acoustic supersoliton and its transition to a regular kind of solitary wave have been explored in detail using Sagdeev pseudopotential technique for a two electron temperature warm multi-ion plasma having two species of ions. It was found that both the cold to hot electron temperature ratio and their respective ambient densities play a deterministic role for the existence of a supersoliton, as well as its transitional processes to a regular solitary wave. Analogous to a double layer solution, which often marks the boundary of the existence domain of a regular solitary wave, a "curve of inflection" determines the boundary of the existence domain of a supersoliton. The characteristics of the "curve of inflection," in turn, depend on the respective concentrations of the two ion species. It is observed that the supersolitons are actually a subset of a more general kind of solutions which are characterized by a fluctuation in the corresponding charge separation which precedes their maximum amplitude. It is also observed that these novel kinds of solitary structures, including supersolitons, occur only for a very narrow range of parameters near constant amplitude beyond which the wave breaks. *Published by AIP Publishing.*
[http://dx.doi.org/10.1063/1.4959851]

I. INTRODUCTION

Earth's magnetosphere is a natural laboratory for studying complex nonlinear plasma waves. From Temerin *et al.*,[1] to recent days CLUSTER multi spacecraft observations, Electrostatic Solitary Waves (ESWs) were widely observed at different magnetospheric boundary layers[2–6] which were often interpreted either as Bernstein, Greene, and Kruskal (BGK) holes[7] or as slow (fast) moving acoustic mode solitary waves driven by ions (electrons).[8–10] It is due to the discontinuity in plasma parameters, instabilities develop at the magnetospheric boundary layers leading to the generation of ESWs. Low altitude slow moving ESWs were often interpreted as Ion Acoustic Solitary Waves (IASWs)[11] and they are known to play crucial roles in particle acceleration processes.[1] Theoretical analyses have shown that the characteristics of such solitary waves often depend on the specific plasma components and their parameters. In Earth's magnetosphere, a multi-component plasma having cooler and hotter electrons is formed by the mixing of hot plasmas of temperature of 100 s eV to few keV, originating in the magnetosphere, and cold plasmas of temperature of few eVs, originating in the ionosphere. On the other hand, the magnetospheric plasma mainly comprises of warm protons (i.e., H^+ ions), with a minority component of heavier species of ions, like α particles (i.e., He^{++} ions), originated from the solar wind, or O^+ ions, introduced from the lower atmosphere and the ionosphere.[12] The study of IASWs in multi-component plasma thus becomes important for understanding the generation and propagation of ESWs. Several authors have previously studied IASWs in a multi-ion plasma model where electrons are either Boltzmann, or assume other nonthermal distributions.[13–19] Though IASWs are well studied and analyzed so far, the recent discovery of super solitary waves or "supersolitons" has renewed the interest in the subject and calls for a revisit of the previous results.

The first signature of a supersoliton can be noted in Baluku *et al.*,[20] where they studied positive amplitude IASWs in two electron temperature cold ion plasma using Sagdeev pseudopotential technique. The particular solution showing the signature of a supersoliton, however, was interpreted as a Regular Double Layer (RDL) rather than any new kind of solution. The concept of the supersoliton was first put forward by Dubinov and Kolotkov[21] who were studying solitary waves for a multi-component plasma containing electrons (e) and positrons (p), along with both positively and negatively charged ion species (epii) or, alternatively, positive ions and negatively charged dust particles (epid). They found that, under some specific conditions, the associated Sagdeev pseudopotential may support three consecutive local extrema, leading to the development of wiggles (knee) like structures in the usual smooth potential profiles of corresponding solutions. This further amounts to the formation of subsidiary extrema on the typical bipolar electric field structures. They termed these structures as "supernonlinear solitons" or "supersolitons" and argued that minimum four component plasma is necessary to support these special kinds of nonlinear structures.

Following Ref. 21, Verheest *et al.*[22] showed that supersolitons may exist in a less complicated situation like a three component plasma comprising positive and negatively charged ions and non-thermal electrons. Verheest *et al.*[23] further studied dust ion acoustic modes in a multi-species plasma comprising stationary negatively charged dust particles, cold fluid ions with positive charges and Cairins non-thermal electrons. They critically compared the

[a]Electronic mail: steffy13@iigs.iigm.res.in
[b]Electronic mail: sukti@iigs.iigm.res.in

characteristics of the associated Sagdeev pseudopotentials and the typical ranges of Mach numbers (or existence domains) for supersolitons, RDLs, and Regular Solitary Waves (RSWs). They have argued that, with coalescence of three local extrema of the Sagdeev pseudopotential, the range of the supersoliton ends. Existence of supersolitons in a three component plasma was further supported by Hellberg *et al.*[24] who studied dust acoustic supersolitons in a three component plasma comprising of negatively charged dust fluid and two non-thermal kappa distributed positive ions. While all these former analyses obtained negative amplitude supersolitons, Maharaj *et al.*[25] have explored the existence domains of both positive and negative amplitude solutions for supersolitons for a four component plasma comprising cold negatively charged dust, warm positively charged dust, non-thermal ions, and Boltzmann electrons. Verheest *et al.*[26] further emphasized that a two component plasma cannot support supersolitons. Rufai *et al.*[27] extended the analysis further to the magnetized plasma. He also worked on its possible applications to the auroral region.[28]

Recently, Ghosh and Iyengar[29] studied positive amplitude IASWs and supersolitons adopting a simple three component plasma model containing warm fluid ions and two temperature Boltzmann electrons. They have shown that both the respective electron concentrations and temperatures play a pivotal role in determining the characteristics of the corresponding solutions. For an appropriate electron temperature ratio, inclusion of extremely low concentration of cooler electron component triggers a positive amplitude RDL solution which in turn, depending on the respective electron parameters, leads to supersolitons. They have identified the specific parameter domains where the respective solutions become significantly different from their regular counterpart. Interestingly, a possible correlation between RDLs and the onset of a supersoliton has also been indicated by Verheest *et al.*[23] In our consecutive works, we intend to focus our attention to such transitional properties of supersolitons in more detail.

So far, supersolitons were defined in terms of the extrema of the Sagdeev pseudopotential which turned the notation entirely technique dependent. Dubinov and Kolotkov[21] have already indicated that supersolitons are non-Kdv type solutions and cannot be obtained by using reductive perturbation method. So a more generalized concept of supersolitons, independent of any particular method, seems to be necessary. In this paper, we are extending the work of Ghosh and Iyengar[29] to a warm multi-ion plasma and two temperature of electrons, obeying Boltzmann distributions. Both the conditions of the onset of supersolitons, as well as its merging to an RSW, have been studied in more detail. It was found that the supersolitons are actually a subset of a more generalized class of solutions which are characterized by a fluctuating charge separation density and are categorically different from the well known RSWs. The actual existence domain of a Regular Supersoliton (RSS), along with the range of its transitional phase to the RSW, has been determined accurately in terms of the charge separation density and its derivatives. The effect of the presence of a minority component of heavier ions has also been explored assuming two different ion concentrations. In this paper, all those different class of solutions are categorized in terms of their Sagdeev pseudopotentials and their derivatives as well as the characteristic fluctuations in their charge separation. The specific roles played by different plasma species, viz., electrons and ions, in determining such special class of solutions have also been explored. It is observed that both the electron temperature and concentrations play deterministic roles in the generation of such solutions.

The present paper has been organized as follows. The model and formulation was explained in Sec. II, while Sec. III explores the existence domain of the supersoliton and its transition to a regular solitary wave parametrically. In Secs. III A and III B, cases of comparatively low and large heavier ion concentration have been considered while Sec. III C compares and summarizes the findings obtained for both the cases. The overall conclusion has been given in Sec. IV.

II. FORMULATION

The plasma is considered to be infinite, homogeneous, collisionless, and unmagnetized, comprising two temperature electrons and two warm ions (lighter and heavier ions). The electrons are obeying Boltzmann distributions and are separately in thermal equilibrium whereas the ions are adiabatic.

The governing normalized fluid equations for the corresponding two warm ions are[30]

$$\frac{\partial n_{il}}{\partial t}+\frac{\partial (n_{il}v_{il})}{\partial x}=0, \tag{1a}$$

$$\frac{\partial n_{ih}}{\partial t}+\frac{\partial (n_{ih}v_{ih})}{\partial x}=0, \tag{1b}$$

$$\frac{\partial v_{il}}{\partial t}+v_{il}\frac{\partial v_{il}}{\partial x}=-Z_{il}\frac{\partial \phi}{\partial x}+3\sigma_l\frac{\partial n_{il}}{\partial x}, \tag{1c}$$

$$\frac{\partial v_{ih}}{\partial t}+v_{ih}\frac{\partial v_{ih}}{\partial x}=-Q\left(Z_{ih}\frac{\partial \phi}{\partial x}-3\sigma_h\frac{\partial n_{ih}}{\partial x}\right), \tag{1d}$$

where the pressure $p_{ij}\propto n_{ij}^{\gamma}(\mathrm{j}=l,\mathrm{h})$, obeying the equation of states, and $\gamma=3$ for the one dimensional adiabatic ions.

In the above equations (Eqs. 1(a)–1(d)), we have

$$\sigma_{eff}=\frac{T_i}{T_{eff}},\quad T_i=\alpha_l T_{il}+\alpha_h T_{ih},\quad T_{eff}=\frac{T_{ec}T_{ew}}{\mu T_{ew}+\nu T_{ec}},$$

where T_i and T_{eff} are the net effective temperature of ions and electrons, respectively. The corresponding Poisson's equation is given as

$$\frac{\partial^2\Phi}{\partial x^2}=n_{ec}+n_{ew}-n_{ih}-n_{il}, \tag{2}$$

with

$$n_e=n_{ec}+n_{ew}=\mu e^{\frac{\Phi}{\mu+\nu\beta}}+\nu e^{\frac{\beta\Phi}{\mu+\nu\beta}}.$$

The subscripts i, e, l, h, c, and w represent ions, electrons, lighter ions, heavier ions, cooler, and warmer electrons, respectively, whereas σ_{eff}, Q, and β refer to the effective temperature ratio of ions $\left(\sigma_{eff}=\frac{T_i}{T_{eff}}\right)$, lighter to heavier ion mass ratio $\left(Q=\frac{m_{il}}{m_{ih}}\right)$,where m_{il} and m_{ih} be the

mass of lighter and heavier ions, respectively, and cold to hot electron temperature ratios $\left(\beta = \frac{T_{ec}}{T_{ew}}\right)$, respectively. Z_{il} and Z_{ih} are the positive electronic charges of lighter and heavier ions, respectively. In this work, we shall consider both the ion species to be singly charged (i.e., $Z_{i(l,h)} = 1$). We have normalized all the number densities n_{il}, n_{ih}, n_{ec}, *and* n_{ew} by the total equilibrium ion density n_0, $(n_0 = n_{ih} + n_{il})$ which in turn gives the corresponding ambient densities as $\alpha_l\left(=\frac{n_{il}}{n_0}\right)$, $\alpha_h\left(=\frac{n_{ih}}{n_0}\right)$, $\mu\left(=\frac{n_{ec}}{n_0}\right)$, and $\nu\left(=\frac{n_{ew}}{n_0}\right)$ for the lighter ions, heavier ions, cooler electrons, and warmer electrons, respectively. The velocities are normalized by the lighter ion acoustic speed $c_{isl}\left(=\sqrt{\left(\frac{T_{eff}}{m_{il}}\right)}\right)$, time by the inverse of lighter ion plasma frequency $\omega_{pil}^{-1}\left(=\left(\frac{n_0 e^2}{\epsilon_0 m_{il}}\right)^{-\frac{1}{2}}\right)$, and lengths by the effective Debye length $\lambda_{eff}\left(=\left(\frac{\epsilon_0 T_{eff}}{n_0 e^2}\right)^{-\frac{1}{2}}\right)$. Pressure $p_{ij}(j = h \quad and \quad l)$ is normalized by the ion equilibrium pressure $p_0(=n_0 T_i)$ and potential ϕ by $\frac{Teff}{e}$.

We undertake the following boundary conditions: $|x| \to \infty$, $v_{ij} \to 0$, $\sum p_{ij} \to 1$, $\sum n_{ij} \to 1$, $\Phi \to 0$, which may also indicate that $p_{ij} \to \alpha_j \frac{\sigma_j}{\sigma_{eff}}$ and $n_{ij} \to \alpha_j$, where $\sigma_j = \frac{T_{ij}}{T_{eff}}, j = l$ and h being the lighter and heavier ions, respectively.

Solving the above fluid equations in the stationary wave frame, $\eta = x - Mt$, where M is the Mach number, we obtain the perturbed densities of ions as[30]

$$n_{il} = \frac{\alpha_l}{2\sqrt{3\sigma_l}}\left[\left(\left(M + \sqrt{3\sigma_l}\right)^2 - 2\Phi\right)^{\frac{1}{2}} - \left(\left(M - \sqrt{(3\sigma_l)}\right)^2 - 2\Phi\right)^{\frac{1}{2}}\right], \tag{3}$$

$$n_{ih} = \frac{\alpha_h}{2\sqrt{3\sigma_h}}\left[\left(\left(\frac{M}{\sqrt{Q}} + \sqrt{3\sigma_h}\right)^2 - 2\Phi\right)^{\frac{1}{2}} - \left(\left(\frac{M}{\sqrt{Q}} - \sqrt{3\sigma_h}\right)^2 - 2\Phi\right)^{\frac{1}{2}}\right]. \tag{4}$$

According to Sagdeev pseudopotential method, we rewrite the Poisson's equation as

$$\frac{\partial^2 \Phi}{\partial \eta^2} = n_i - n_e = -\frac{\partial \Psi(\Phi)}{\partial \Phi}, \tag{5a}$$

$$\text{which leads to,} \quad \frac{1}{2}\left(\frac{\partial \Phi}{\partial \eta}\right)^2 + \Psi(\Phi) = 0, \tag{5b}$$

where $\Psi(\Phi)$ is the Sagdeev pseudopotential.

Integrating the Poisson's equation (Eq. (5a)) with the ion densities and electron densities, we got the corresponding Sagdeev pseudopotential as

$$\begin{aligned}\psi(\Phi) = -\Bigg[&(\mu + \nu\beta)\left\{\mu\left(\exp\frac{\Phi}{\mu + \nu\beta} - 1\right) + \frac{\nu}{\beta}\left(\exp\frac{\beta\Phi}{\mu + \nu\beta} - 1\right)\right\} \\ &+ \frac{\alpha_l}{6\sqrt{3\sigma_l}}\left\{\left[\left(M + \sqrt{3\sigma_l}\right)^2 - 2\Phi\right]^{\frac{3}{2}} - \left(M + \sqrt{3\sigma_l}\right)^3 - \left[\left(M - \sqrt{3\sigma_l}\right)^2 - 2\Phi\right]^{\frac{3}{2}} + \left(M - \sqrt{3\sigma_l}\right)^3\right\} \\ &+ \frac{\alpha_h}{6\sqrt{3\sigma_h}}\left\{\left[\left(\frac{M}{\sqrt{Q}} + \sqrt{3\sigma_h}\right)^2 - 2\Phi\right]^{\frac{3}{2}} - \left(\frac{M}{\sqrt{Q}} + \sqrt{3\sigma_h}\right)^3 - \left[\left(\frac{M}{\sqrt{Q}} - \sqrt{3\sigma_h}\right)^2 - 2\Phi\right]^{\frac{3}{2}} + \left(\frac{M}{\sqrt{Q}} - \sqrt{3\sigma_h}\right)^3\right\}\Bigg].\end{aligned} \tag{6}$$

In order to obtain solitary wave solution, Eq. (6) has to satisfy the following conditions:

$$\Psi(\Phi = 0) = \frac{\partial \Psi}{\partial \Phi} = 0; \quad \frac{\partial^2 \Psi(0)}{\partial \Phi^2} < 0;$$
$$\Psi(\Phi_0) = 0; \quad \frac{\partial \Psi(\Phi_0)}{\partial \Phi} \neq 0. \tag{7}$$

This also implies that $\Psi(\Phi) < 0$ for $0 < |\Phi| < |\Phi_0|$, where Φ_0 is the amplitude of the solitary waves.

For an RDL, apart from the above mentioned conditions (Eq. (7)), the following conditions:

$$\Psi(\Phi_d) = 0; \quad \frac{\partial \Psi(\Phi_d)}{\partial \Phi} = 0, \tag{8}$$

also need to be satisfied where Φ_d is the amplitude of the RDL. For our model, the compressive positive amplitude solitary wave should further satisfy the energy condition given by

$$\Phi_0 < \frac{1}{2}\left(M - \sqrt{(3\sigma_l)}\right)^2, \tag{9}$$

beyond which $\Psi(\Phi)$ becomes complex and the wave breaks.

These conditions have been further illustrated in Figs. 1(a) and 1(b) which show an RSW and RDL, respectively. An RSW has two roots (points 1 and 2 in Fig. 1(a))

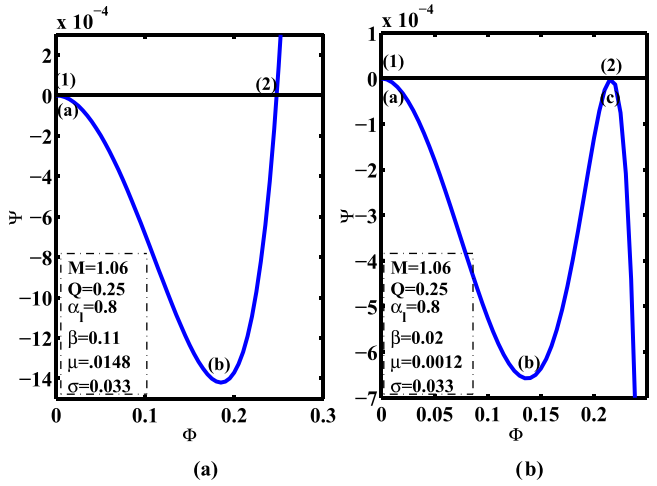

(a) (b)

FIG. 1. Sagdeev pseudopotentials for (a) IASW and (b) RDL, respectively.

and two extrema (points a and b, in Fig. 1(a)), whereas a RDL has two roots like a solitary wave (points 1 and 2, in Fig. 1(b)) but three extrema (points a, b, and c, in Fig. 1(b)), respectively.

III. RESULTS AND DISCUSSION

According to the previous studies by Ghosh and Iyengar,[29] occurrence of a forbidden region in μ, the minority cooler electron concentration, is a necessary condition for the existence of supersolitons though it is not sufficient. They have further shown that the electron temperature ratio (β) may play a deterministic role for both the onset of supersolitons and the said forbidden regions. The transition of a supersolitary wave to a regular IASW is, however, still not well known. Thus, in the present work, we intend to study the effect of β on the existence domain of supersolitons in more detail. We have also generalized the previous model by assuming two singly charged ion populations for our plasma. For the sake of our convenience, it is assumed that both the heavier and lighter ions are of same temperatures, i.e., $\sigma_l = \sigma_h = \sigma$, and it remains constant (i.e., $\sigma = 1/30$) throughout our analysis. It is also assumed that the plasma is mainly comprised of H^+ ions with a minority component of He^+ ions, keeping the mass ratio $Q(= 1/4)$ a constant. To establish our findings, we considered two different concentrations of heavier ions, namely, $\alpha_h = 0.1$ (low) and $\alpha_h = 0.2$ (high), respectively. For the sake of comparison, we have also kept the Mach number constant ($M = 1.06$).

Following Ghosh and Iyengar,[29] we have plotted the variation of amplitude (Φ_0) with μ in Fig. 2 for two different β values, keeping the concentration of the minority components of heavier ions a constant (i.e., $\alpha_h = 0.2$). The lower curve (curve 1), with larger β value ($\beta = 0.2$), is continuous and depicts a smooth transition from two electrons to a single electron temperature plasma whereas the upper curve (curve 2) with lower $\beta(\beta = 0.07)$ shows forbidden regions in μ. It further indicates that the parameter regime associated with curve 1 comprises with RSWs only, whereas that associated with curve 2, particularly the left hand side of the curve, (i.e., the low $\beta - \text{low}\mu$ regime), may also exhibit

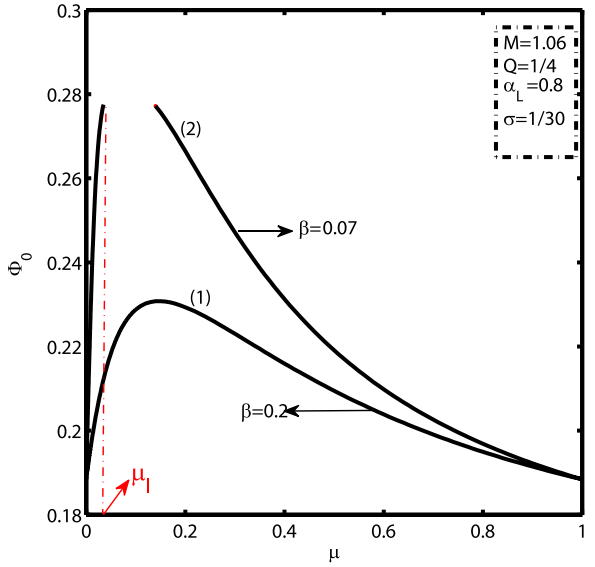

FIG. 2. Variation of amplitude of the IASW (Φ_0) with respect to the cooler electron concentration (μ) for two different values of β.

supersoliton solutions.[29] While RSWs are well studied by many authors,[14–16] the latter one (i.e., curve 2) has received a scant attention so far and needs a closer look. The onset of the forbidden region is further characterized by a limiting value of μ, viz., $\mu = \mu_l$, as shown in Fig. 2, beyond which the solitary wave solutions terminate for the low $\beta - \text{low}\mu$ regime. This further implies that the existence domain of supersolitons is expected to be bounded by the parameter regime of $\mu \leq \mu_l$.

To illustrate the effect of β on various genre of nonlinear structures, viz., RSWs, RDLs, and RSSs, we have plotted the variation of Φ_l with β in Fig. 3 for both single (dashed line) and multi-ion (solid line) plasmas where Φ_l is the corresponding amplitude for that particular value of $\mu = \mu_l$ (i.e., $\Phi_l = \Phi_0(\mu_l)$, Φ_0 being the IASW amplitude), whereas Φ_d corresponds to the amplitude of RDLs, and all other parameters are kept constant. It readily shows two distinct regions, viz., A and B, and the boundary of these two regions is defined by the parameter $\beta = \beta_f$ where β_f is the largest β

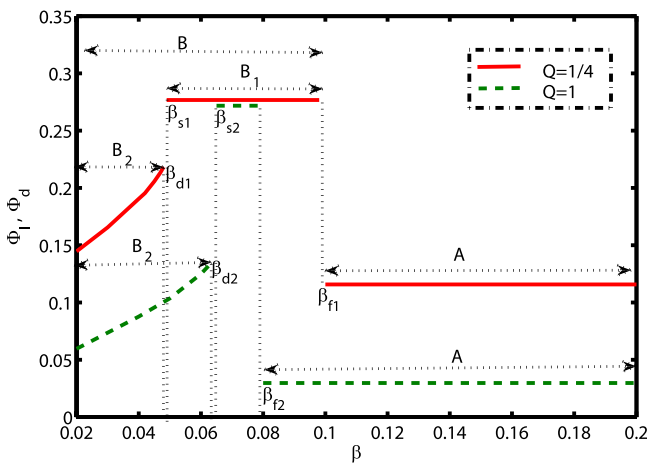

FIG. 3. The variation of Φ_l (regions A and B1) and Φ_d (region B2) with respect to β for two different Q values.

value associated with the forbidden regions in μ. For region A, which may be defined as $\beta > \beta_f$, the limiting value of μ_l goes to 1, i.e., single electron temperature plasma, whereas for region B (i.e., $\beta \leq \beta_f$), it terminates at sufficient low value of μ (e.g., curve 2 in Fig. 2). Figure 3 shows that, compared to a single ion solution (dashed line), β_f shifts to a higher value for multi-ions (solid line), indicating that the range of parameters supporting forbidden regions may increase with the inclusion of a heavier ion species. A more detailed analysis in this regard is currently under process and will be communicated elsewhere.

A closer look to Fig. 3 readily shows that region B is sharply divided into two subregions, namely, B_1 and B_2, where the boundary is marked by a steep discontinuity in the variation of amplitude. In region B_2, the solitary wave solutions are known to be terminated to a Regular Double Layer (RDL) as shown in Fig. 1(b). The region thus comprises of both RSWs and RDLs and may be parametrically defined as $\beta \leq \beta_d$ where β_d is the largest β value supporting compressive RDLs (Fig. 3).

While both regions A and B_2 show regular solutions, i.e., RSWs and RDLs, region B_1 is marked with the onset of supersolitons and may be defined as $\beta_s \leq \beta \leq \beta_f$, where β_s is the lowest β supporting supersolitons for the selected parameter regime (Fig. 3). With the inclusion of multi-ions, the value of both β_d and β_s shift to a lower value of β while β_f increases. In other words, inclusion of a heavier ion species tends to increase the range of region B_1. Compared to region B_2, which shows a slow but steady increase in amplitude with β, it remains almost constant in region B_1.

It is known that, for an RSW (RDL), the associated Sagdeev pseudopotential curve shows two (three) extrema and two roots as shown in Figs. 1(a) and 1(b). On the other hand, RSSs are, so far, defined as solitary wave solutions with four extrema and two roots of the corresponding Sagdeev pseudopotential profiles and are known to merge gradually to an RSW.[23,29] In other words, at its low β end (i.e., towards β_s), region B_1 comprises RSSs, while at the large β end (i.e., towards β_f), it has RSWs only. The region also exclusively comprises the transitional phase in between RSSs and RSWs. Verheest *et al.*[23] have previously indicated that such transitions occur due to merging of the two consecutive extrema. To understand it in more detail, we considered four snapshots in region B1 and replicated our analyses for two values of α_h (=0.1 and 0.2, respectively). The details are as follows.

A. Case I: Low $\alpha_h(\alpha_h=0.1)$

We have considered a plasma model with a comparatively smaller heavier ion concentration, (i.e., $\alpha_h = 0.1$) while all other ionic parameters (viz., $\sigma = \frac{1}{30}$, and $Q = \frac{1}{4}$) and the Mach number $(M = 1.06)$ remained the same as mentioned in Fig. 3. We have chosen four convenient values of β for our analysis and μ is assumed to be the corresponding μ_l for each β value. Figs. 4(a)–4(d) show the four snapshots of the Sagdeev pseudopotentials for the chosen β values. Figs. 4(a) and 4(d) represent an RSS and RSW, respectively, while Figs. 4(b) and 4(c) show the transitional phases between an RSS and RSW. The points (i) and (ii) in the figures represent the roots of the respective pseudopotentials (i.e., $\Psi(\Phi) = 0$), while points 1, 2, 3, etc., mark the extrema of the curve where its slope changes its sign. All the four curves in Figs. 4(a)–4(d) show two roots only and hence represent generalised solitary wave solutions. A closer inspection, however, reveals significant differences in their pseudopotentials. Unlike an RSW (Fig. 4(d)), which has a smooth profile, Figs. 4(a)–4(c) show significant variations or fluctuations of the curves and may thus be categorized as a

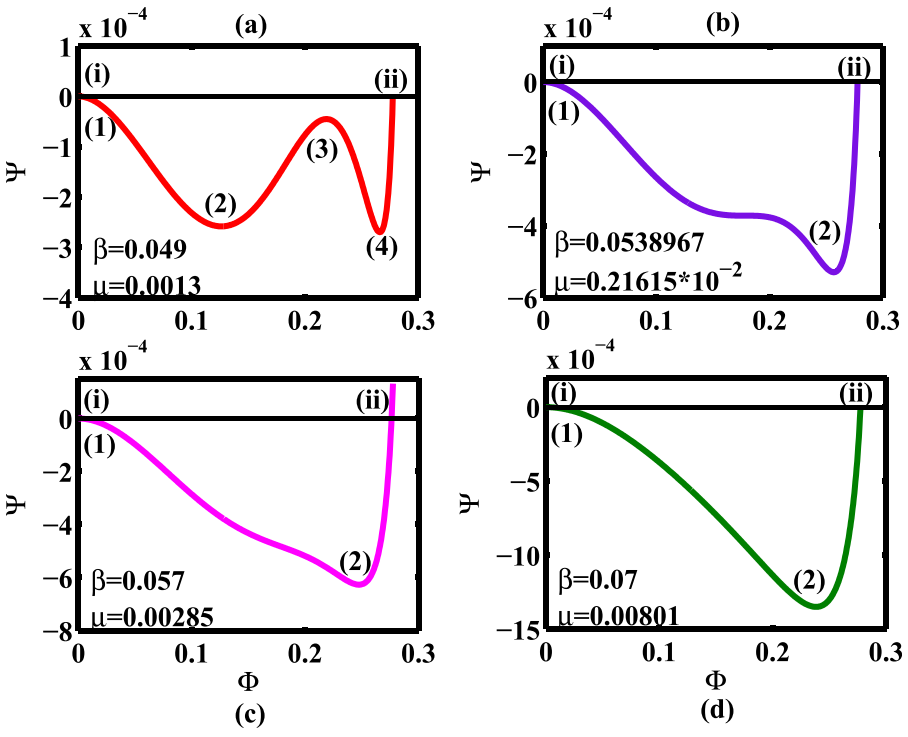

FIG. 4. Snapshots of Sagdeev pseudopotentials for corresponding β values representing different nonlinear structures, viz., (a) RSS, (b) curve of inflection, (c) generalized VSW, and (d) RSW; $\alpha_h = 0.1$.

fluctuating or Variable kind of Solitary Waves (VSWs). On the other hand, except Fig. 4(a) (i.e., an RSS), which shows 4 extrema for the curve (viz., points 1 to 4), all other curves (Figs. 4(b)–4(d)) exhibit only two extrema and hence none of them can be termed as an RSS.

Noting the importance of the slope (i.e., $\frac{\partial\Psi}{\partial\Phi}$), and remembering that the slope of a Sagdeev pseudopotential represents the charge separation density (Eq. (5a)), we explored the variation of different order of derivatives of the Sagdeev pseudopotential with Φ. In order to understand the deviations of Figs. 4(b) and 4(c) from Fig. 4(a) in one hand and Fig. 4(d) from the other, we have plotted the variation of the slope of the corresponding pseudopotential profiles with Φ (Fig. 5). According to Eq. (5a), the slope of the pseudopotential is the measure of the charge separation, $\Delta n = n_i - n_e$. Consequently in Fig. 5, curves 1 (solid line), 2 (dashed and dotted line), 3 (dotted line), and 4 (dashed line) correspond to the variation in charge separation (Δn) with respect to potential (Φ) for the pseudopotential profiles in Figs. 4(a)–4(d), respectively. It shows that curve 1, which corresponds to an RSS, has four roots, (i.e., $\frac{\partial\Psi}{\partial\Phi} = 0$), curve 2 has three roots while curves 3 and 4 (RSW) have only two roots each including the origin. Each of these roots clearly represents the corresponding extrema, marked by (i), (ii), etc., in Figs. 4(a)–4(d). As indicated earlier, the first three curves (viz., curves 1–3) show significant fluctuations in the Δn, and so we propose to club them together under the label "Variable Solitary Waves" (VSW). Therefore, RSS (curve 1) becomes a subset of a more general class of solutions like VSWs. Contrary to them, for curve 4 corresponding to RSW, Δn first decreases and then increases monotonically with increasing Φ without any fluctuations. Interestingly, in the case of curve 2, not only $\Delta n\left(=\frac{\partial\Psi}{\partial\Phi}\right)$ but also its derivative $\frac{\partial\Delta n}{\partial\Phi}\left(=\frac{\partial^2\Psi}{\partial\Phi^2}\right)$ become zero at the point $\Phi = \Phi_{infl}$ which implies a point of inflection for the associated Sagdeev pseudopotential (Fig. 4(b)). Defining $\beta = \beta_{infl}$ for curve 2, the curve of inflection, and following the trend of the curves in Fig. 5, it becomes evident that, for any $\beta > \beta_{infl}$, the net number of roots (or extrema in Figs. 4(a)–4(d)) will be less than 3 (<3) while for $\beta > \beta_{infl}$ it will be greater than 3 (>3), curve 2 being the limiting profile for both the regime. This further implies that the existence domain of an RSS is bounded by $\beta < \beta_{infl}$ where β_{infl} eventually marks the onset of the transitional phase between RSS and RSW. Noting that β_s has marked the onset of RSS (Fig. 3), the existence domain of an RSS can now be precisely defined as $\beta_s \le \beta < \beta_{infl}$, beyond which it ceases to exist. Fig. 5 further shows that, for $\beta \ge \beta_{infl}$, the fluctuation of the overall charge separation density always remain negative (i.e., $n_e > n_i$) except near the maximum amplitude.

In Figs. 6(a) and 6(b), we have plotted the subsequent 2nd and 3rd order derivatives of the pseudopotential, respectively, while all the legends remain the same as earlier. In Fig. 6(a), curves 1–3 show fluctuations with 3 roots each $(\frac{\partial^2\Psi}{\partial\Phi^2} = 0)$ while curve 4 is monotonic with only one root. This further clarifies the differences between RSWs and VSWs where an RSS is a special case of the latter. The 2nd root of curve 2 in Fig. 6(a) coincides with that of Fig. 5 determining the "point of inflection" at $\Phi_{infl} = 0.2768$ while the estimated value of the corresponding $\beta_{infl} = 0.0538967$ for our present set of parameters.

Figure 6(b) further shows the variation of the third derivatives where curves 1–3 fluctuate between positive and negative values, having two roots each, but curve 4 remains always positive without any root. This defines another limiting value of $\beta = \beta_v, \beta_v$ being the maximum β value which supports a negative $\frac{\partial^3\Psi}{\partial\Phi^3}$ for the solution. For any $\beta > \beta_v$, the solution is an RSW only. The estimated value of β_v for the present case is 0.067.

So far we have discussed different genre of solitary waves which are associated with variant characteristics of Sagdeev pseudopotential profiles and their derivatives. This in turn indicates a significant role played by the

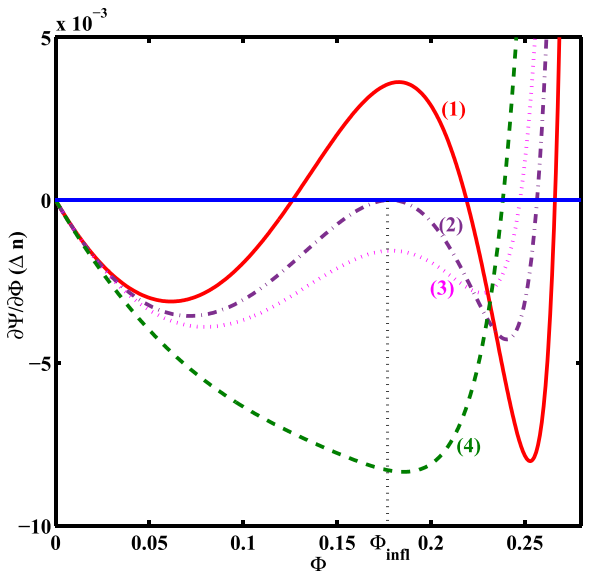

FIG. 5. Variation of charge separation Δn with potential Φ for $\alpha_h = 0.1$.

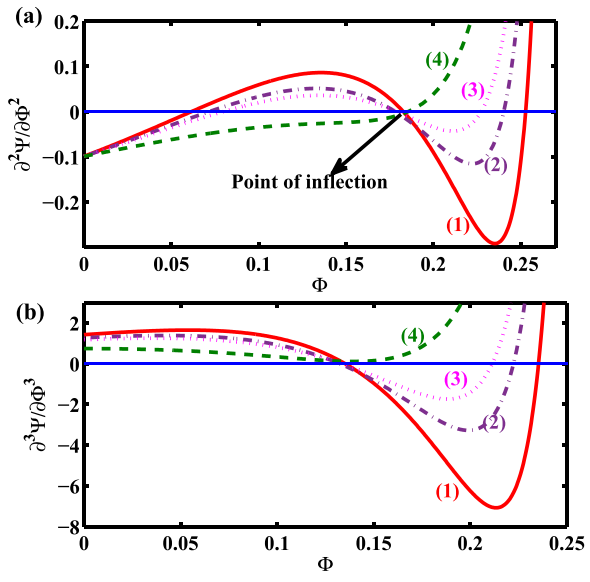

FIG. 6. Variations of (a) $\frac{\partial^2\Psi}{\partial\Phi^2}$ and (b) $\frac{\partial^3\Psi}{\partial\Phi^3}$ with potential Φ for $\alpha_h = 0.1$.

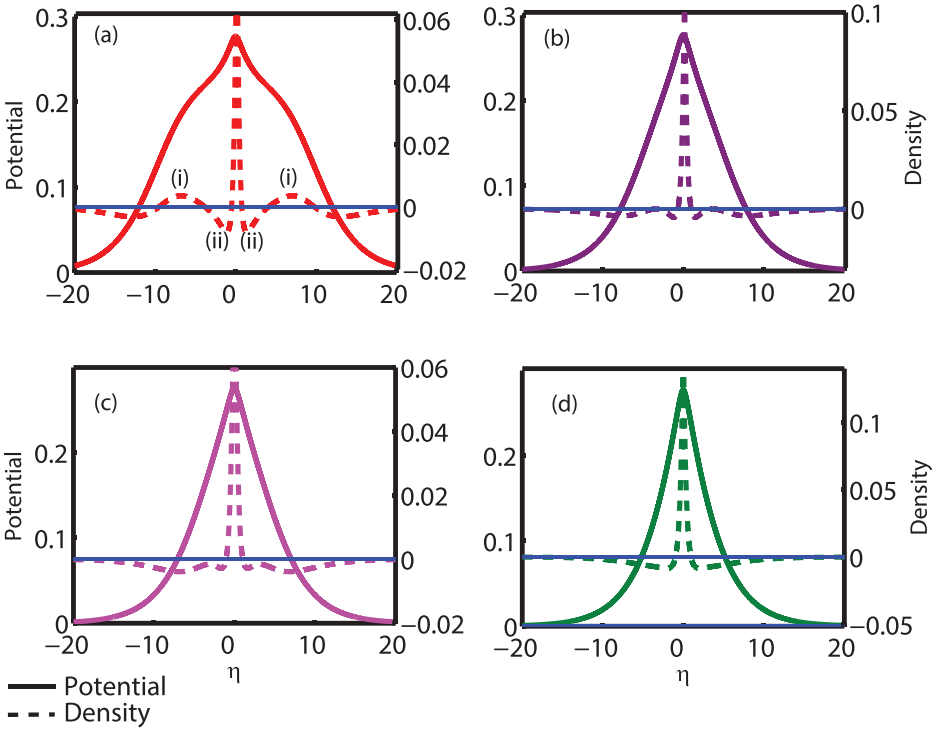

FIG. 7. The potential profiles (solid line) and density profiles (dashed line) corresponding to different nonlinear structures, viz., (a) RSS, (b) the curve of inflection, (c) generalized VSW, and (d) RSW; $\alpha_h = 0.1$.

corresponding Δn. To estimate its actual contribution, we have plotted the potential profiles (solid lines) and their associated $\Delta n = n_i - n_e$(dashed lines) in Figs. 7(a)–7(d) where the potential profiles have been determined by solving Eq. (5b) numerically for the Sagdeev pseudopotentials shown in Figs. 4(a)–4(d), respectively, and all the corresponding Δn have been calculated analytically using Eq. (5a). In Fig. 7(a), point (i) shows a positive, $(n_i > n_e)$, or compressive Δn while at point (ii) it becomes negative $(n_i < n_e)$, or rarefactive. The overall potential profile remains positive representing a compressive RSS. The characteristic wiggle in the potential profile of the RSS appears at the very point where Δn oscillates from positive to negative. Therefore in the case of RSSs, we have alternate compressions and rarefactions within the overall compressive potential structure where the fluctuations in Δn lead to the generation of wiggles in the corresponding potential profiles. An initial oscillation in Δn from a positive to a negative value can thus be considered as an alternate and independent definition of a regular compressive supersoliton. From the RSS (Fig. 7(a)), as we approach to a more generalised VSW solution (Figs. 7(b) and 7(c)), the Δn fluctuation diminishes and consequently the wiggles in the potential profiles, too, gradually smoothen. In Fig. 7(b), though the fluctuation remains fairly significant,

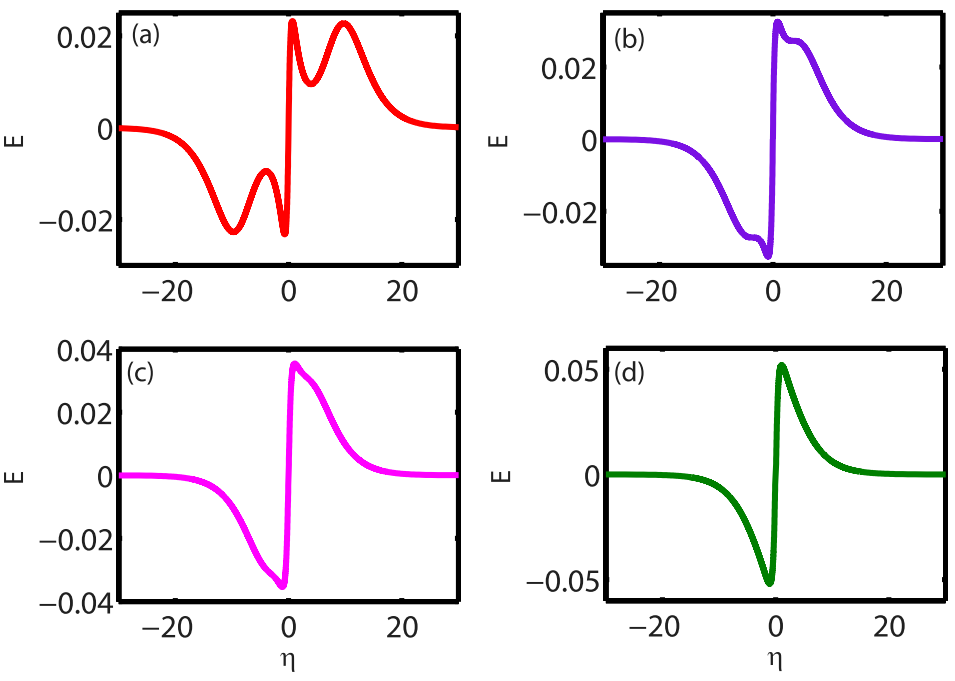

FIG. 8. The electric field (E field) profiles corresponding to different nonlinear structures, (a) RSS, (b) the curve of inflection, (c) VSW, and (d) RSW; $\alpha_h = 0.1$.

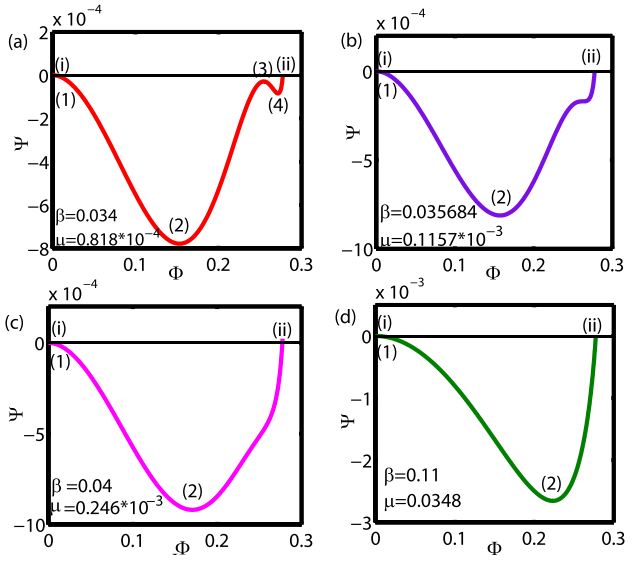

FIG. 9. Snapshots of Sagdeev pseudopotentials for corresponding β values representing different nonlinear structures, viz., (a) RSS, (b) curve of inflection, (c) generalized VSW, and (d) RSW; $\alpha_h = 0.2$.

it ceases to oscillate to a negative value, keeping $\Delta n > 0$ $(n_i > n_e)$. The profile comprises the "point of inflection" as described in Fig. 4(b) and curve 2 in Fig. 5. Both the fluctuation in Δn and the wiggle in the potential profile diminish further in Fig. 7(c) while Fig. 7(d) shows a smooth profile for both the potential and Δn, representing a regular compressive IASW.

To compliment Figs. 7(a)–7(d), we have plotted the corresponding electric field profiles in Figs. 8(a)–8(d), respectively, which subsequently represent the RSS (Fig. 8(a)), the VSW for the curve of inflection (Fig. 8(b)), the generalised VSW apart from the aforementioned two (Fig. 8(c)), and the RSW (Fig. 8(d)) solutions. This further confirms that the extra wiggles in the bipolar structure of the RSS (Fig. 8(a)) are formed due to the fluctuations in Δn. A similar correlation has also been reported by Hellberg *et al.*[24] for a dust acoustic supersoliton in a plasma with negative dust grains and two

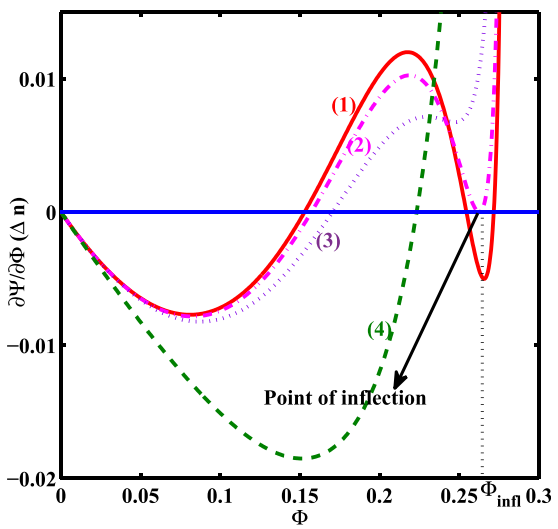

FIG. 10. Variation of charge separation density (Δn) with potential Φ for $\alpha_h = 0.2$.

kappa distributed ions. They termed it as a seven layer structure in the profile of Δn. In his work, he also pointed out the role of Δn fluctuations in electric field profile as we observed in Fig. 8(a). Figures 8(a)–8(d) clearly show that the prominence of extra wiggles in a typical bipolar electric field structure diminishes as we proceed from RSS to RSW.

B. Case II: High α_h(α_h=0.2)

We have revisited the above observations by varying the heavier ion concentration to a higher value $(\alpha_h = 0.2)$. For this value of α_h, once again, we have four "snapshots" of Sagdeev pseudopotential profiles, shown in Figs. 9(a)–9(d) while Fig. 10 shows the corresponding variations of their slopes with Φ. Even though both the profiles (Figs. 9 and 10) confirm the aforementioned observations in Sec. III A, we can notice a significant change in the morphology of the Sagdeev pseudopotential profile (Fig. 9(b)) and charge separation Δn (curve 2 in Fig. 10) for the inflection point. Figures 11(a)–11(d) summarize all the variations near the point of inflection where, for the sake of comparison, we have plotted the corresponding Sagdeev pseudopotentials (Figs. 11(a) and 11(b)) and their associated variations of the charge separations (Figs. 11(c) and 11(d)) for two values of α_h, viz., $\alpha_h = 0.1$ (Figs. 11(a) and 11(c)), and $\alpha_h = 0.2$ (Figs. 11(b) and 11(d)), respectively. As the heavier ion concentration (α_h) increases from 0.1 to 0.2, the point of inflection shifts from the first subwell (Fig. 11(a)) to the second (Fig. 11(b)). Accordingly, variation of the Δn near the point of inflection $(\Phi = \Phi_{infl})$ turns from a maxima (Fig. 11(c)) to a minima (Fig. 11(d)). In other words, while the Δn near the vicinity of Φ_{infl} remains negative for a low α_h, it turns positive when α_h increases to a higher value. Since for $\alpha_h = 0.1$, the Δn curve (Fig. 11(c)) shifts to the negative regime, hence, for our convenience, we represent the corresponding value of β_{infl} as β^n_{infl}. Similarly, for $\alpha_h = 0.2$, the Δn curve (Fig. 11(d)) shifts

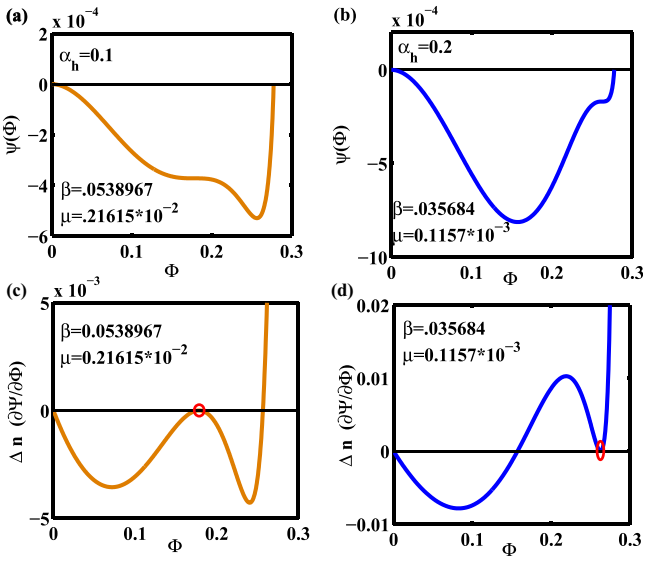

FIG. 11. (a) Sagdeev pseudopotential profile corresponding to $\beta = \beta_{infl}$ for $\alpha_h = 0.1$, (b) Sagdeev pseudopotential profile corresponds to $\beta = \beta_{infl}$ for $\alpha_h = 0.2$, (c) charge separation density profile at $\beta = \beta_{infl}$ for $\alpha_h = 0.1$, and (d) charge separation density profile at $\beta = \beta_{infl}$ for $\alpha_h = 0.2$.

to the positive regime of Δn and hence the corresponding value of β_{infl} is represented as β^p_{infl}. Despite the changes in the morphology of the Sagdeev pseudopotential, and the shift in the Δn curve, the solution associated with the "point of inflection" continues to be the boundary for an RSS. From Fig. 10, it can also be observed that, as curve 2 (i.e., the curve with inflection) shifts, all other curves between RSS and RSW also shift accordingly. This further indicates that the presence of a heavier ion species may significantly modify the morphology of the boundary curve (charge separation curve with point of inflection) and hence may affect the existence domain of the supersoliton.

Following Sec. III A, we have also plotted the variations of the second $\left(\frac{\partial^2\Psi}{\partial\Phi^2}\right)$ and third derivatives $\left(\frac{\partial^3\Psi}{\partial\Phi^3}\right)$ of Ψ with Φ as shown in Figs. 12(a) and 12(b), respectively. The curves follow the same trend as observed in Sec. III A. From Fig. 12(a), we have estimated the inflection parameters as $\Phi_{infl} = 0.2768$ and $\beta^p_{infl} = 0.035684$ while Fig. 12(b) determines the value of $\beta_v = 0.04$. It shows that, with an increase in the heavier ion concentration, the corresponding value of β_{infl} and β_v decreases.

Figures 13(a)–13(d) show the potential profile (solid lines) and the charge separation (Δn, dashed line) corresponding to each pseudopotential curve represented in Figs. 9(a)–9(d), respectively. While the qualitative trend remains the same as Sec. III A, the extent of oscillations turns to be far more prominent in the present case. Thus for a regular supersoliton, after a large initial compression, we observe a comparatively small scale of rarefaction, followed by another sharp increase in Δn leading to its maximum amplitude (Fig. 13(a)). The significant drop in Δn indicates alternate compressions and rarefactions within the overall compressive structure. The wiggles in the potential profile arise in the region where we have sudden fluctuations in Δn. The overall profile of Δn in Fig. 13(a) closely resembles to the aforementioned seven layer structures observed by

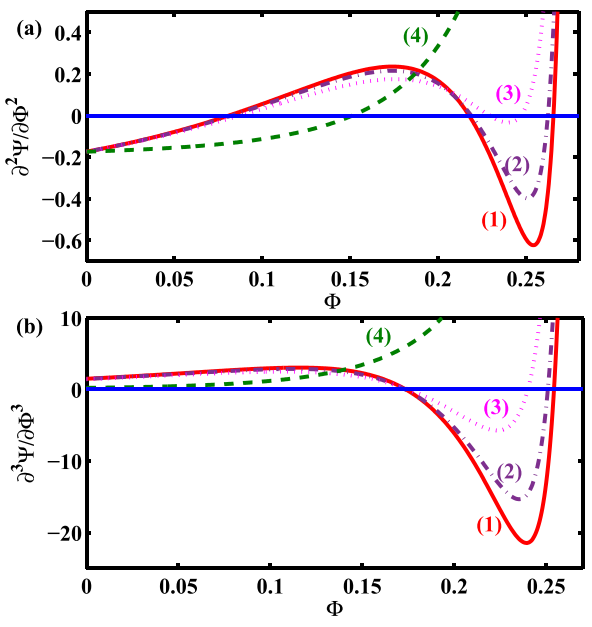

FIG. 12. Variation of (a) $\frac{\partial^2\Psi}{\partial\Phi^2}$ and (b) $\frac{\partial^3\Psi}{\partial\Phi^3}$ with potential Φ for $\alpha_h = 0.2$.

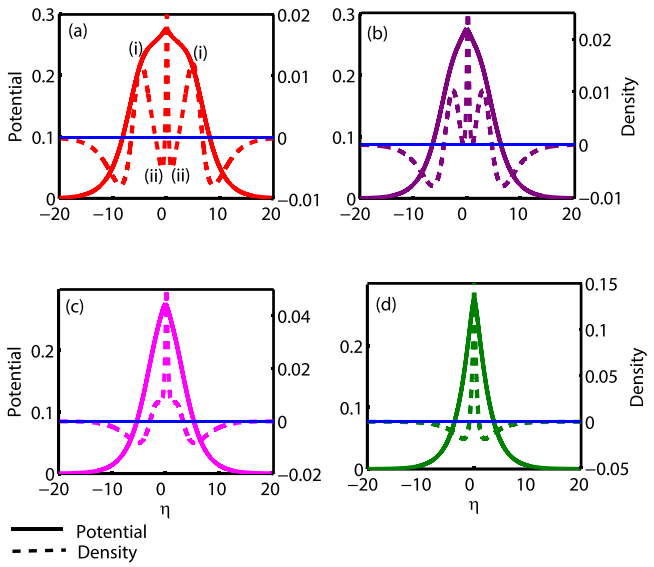

FIG. 13. The potential profiles (solid line) and density profiles (dashed line) corresponding to different nonlinear structures, viz., (a) RSS, (b) the curve of inflection, (c) generalized VSW, and (d) RSW; $\alpha_h = 0.2$.

Hellberg *et al.*[24] because of its extra large fluctuations compared to that for the previous case (Fig. 7(a)). As the solution approaches to RSWs, the fluctuations in Δn diminishes, which eventually results in the formation of a smooth potential profile as shown in Fig. 13(d). In Figs. 14(a)–14(d), we plotted the electric field corresponding to each potential profile depicted in Figs. 13(a)–13(d), respectively. This further confirms that the wiggles in the bipolar electric field of an RSS appear due to its fluctuation in the Δn.

C. Regime of nonlinear structures

Sections III A and III B revealed finer structures of region B_1 (Fig. 3) which are defined by different characteristic β values. In Fig. 15, we have plotted the variation of

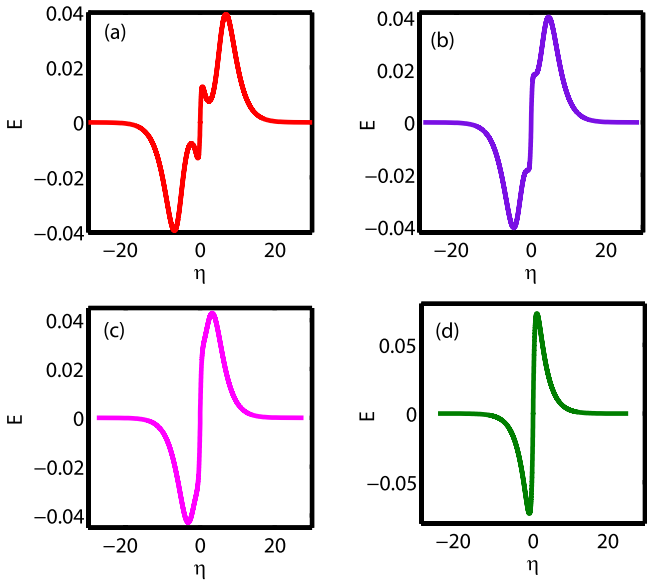

FIG. 14. The electric field (E field) profiles corresponding to different nonlinear structures: (a) RSS, (b) the curve of inflection, (c) VSW, and (d) RSW; $\alpha_h = 0.2$.

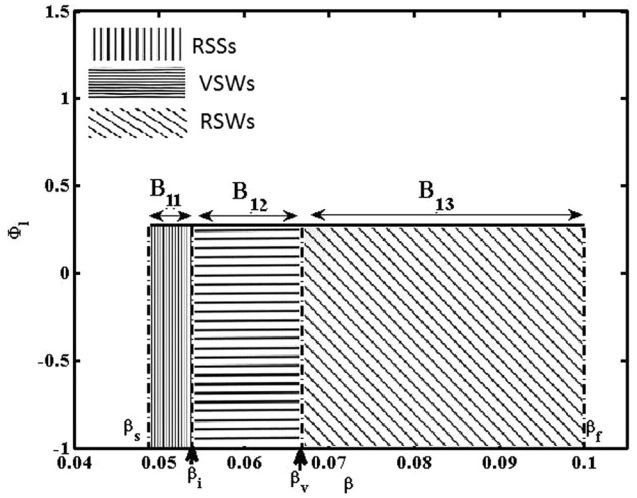

FIG. 15. The regime of nonlinear structures, region B_{11} represents RSS, region B_{12} represents transition region and region B_{13} corresponds to RSWs: $\alpha_h = 0.1$.

amplitude (Φ_l) with β for different nonlinear structures in region B_1. As we have mentioned earlier, the overall region is bounded by the parameters β_s and β_f, respectively, where the former represents the onset of the RSS and the latter denotes the disappearance of the "forbidden region" beyond it. The parameter β_{infl} denotes the boundary for the RSS solution and the subregion B_{11}, shaded by vertical lines in Fig. 15 and bounded between β_s and β_{infl} (i.e., $\beta_s \leq \beta < \beta_{infl}$) represents the RSS existence domain. The next subregion B_{12}, shaded by horizontal lines, represents the transitional phase between RSS to RSW and bounded between β_{infl} and β_v (i.e., $\beta_{infl} \leq \beta \leq \beta_v$). All the solutions in these subregions are VSWs but there is no RSS. Regions B_{11} and B_{12} together represent the existence domain of all VSWs, including RSSs, and is bounded between β_s and β_v, (i.e., $\beta_s \leq \beta \leq \beta_v$). The parameter β_v marks the boundary of any kind of VSWs and the subregion B_{13}, which lies beyond $\beta_v(\beta > \beta_v)$ and shaded by slanted lines (Fig. 15), comprises RSWs only. Technically, the solitary wave solutions in the subregion B_{13} are the same as that of region A in Fig. 3, though for the former there still occur forbidden regions for a range of μ values. Even though the structure and morphology of the nonlinear structures vary, and although both β and μ vary significantly over the range, the amplitude (Φ_l) of all these nonlinear structures over region B1 remains almost constant. A closer inspection reveals that, throughout the region B1, the corresponding amplitude Φ_l for the limiting value of $\mu = \mu_l$ is only marginally smaller than the terminating amplitude $\phi_t \left(= \frac{1}{2}\left(M - \sqrt{(3\sigma_l)}\right)^2 \right)$ (Eq. (9)) of the system. It further indicates that all the VSWs and supersolitons occur due to a very fine balance of their parameters beyond which either the wave breaks, or collapses to a far smaller amplitude RSW solutions (region B2 in Fig. 3). This also highlights the deterministic role played by the electron temperature ratio (β). Table I summarizes all the characteristics β and the relevant regimes while Table II summarizes their estimated values for our chosen set of parameters.

TABLE I. Definition of parameters and regime.

Parameter	Definition	Regime
β_s	Smallest β for RSS	$\beta_s \leq \beta \leq \beta_f$ (region B_2 in Fig. 3)
β_f	Largest β for forbidden region	
β_{infl}	β at the point of inflection	$\beta_s \leq \beta < \beta_{infl}$ (region B_{11}) Existence domain of RSS
β^p_{infl}	β value corresponds to positive inflection (Fig. 11(b))	
β^n_{infl}	β value corresponds to negative inflection (Fig. 11(a))	
β_v	Largest β for VSWs	$\beta_s \leq \beta < \beta_v$ region for RSSs + VSWs $\beta_{infl} \leq \beta < \beta_v$ transitional phase $\beta < \beta_v$ region for RSWs

TABLE II. Value of parameters.

Parameters	$\alpha_h = 0.1$	$\alpha_h = 0.2$
β_s	0.049	0.034
β_{infl}	0.0538967	0.035684
β_v	0.067	0.04
β_f	0.1	0.09

IV. CONCLUSION

In this paper, we considered a four component plasma, consisting of two electrons and two ions. As we have observed earlier,[29] the nonlinearity associated with the secondary electron species caused the generation of compressive double layers and RSS. Interestingly, apart from the electronic parameters, it was found that the presence of the minority component of heavier ions modify the boundary condition for a supersoliton solution. One major achievement of our work is to precisely quantify the existence domain of the RSS in terms of electron temperature ratio (β). It is observed that, as the heavier ion concentration (α_h) increases, the curve of inflection turns positive to negative, thus changing the boundary condition for the supersoliton.

After detailed analysis, we found that there exists a new class of nonlinear structures beyond the RSS which are categorically different from the well known regular solitary waves (RSWs) and, like the RSS, identified by a characteristic type of fluctuations in the charge separation density (Δn). We proposed to call them as variable solitary wave (VSWs) because of their variability in the Δn. We found that RSSs are a subset of VSWs where the fluctuations in Δn actually changes sign. In other words, a compressive supersoliton may be defined as a compressive solitary wave structure where the overall compression of the ion density is preceded by a fluctuation of compressive to rarefactive ion density. It is this fluctuation in the Δn which manifests itself in producing subwells in the corresponding pseudopotential profile and leads to the observed wiggles in the otherwise bipolar electric field. Such fluctuations are totally absent for any RSW which further marks the aforementioned solutions

(VSWs) as unique. The resulting correlation between the fluctuation of Δn and the wiggle in the electric field was also identified by Hellberg *et al.*[24] which further supports our findings.

While the curve of inflection determines the boundary of RSS, it also marks the onset of the transitional phase between an RSS and RSW. The solutions in this regime still show prominent fluctuations and can thus rightly called as VSWs but, unlike RSS, the Δn ceases to be negative. In other words, there is no preceding rarefaction before it grows to its maximum amplitude. Interestingly, as the heavier ion concentration increases, not only the morphology of the curve of inflection changes but also the intensity of the fluctuations increases many fold. Hellberg *et al.*[24] termed such kinds of solutions as seven layers for those observed "folds" in the overall profile of the Δn.

In the present work, we were interested to study the transitional properties of the RSS and hence we concentrated only on region B1. For the sake of convenience, we restricted our analysis to only the limiting value solutions where the resulting amplitude Φ_l remains very close to the terminating amplitude, beyond which the wave breaks. Moreover, the limiting amplitude Φ_l is determined for the limiting value of $\mu = \mu_l$ which further marks the onset of forbidden regions. This eventually makes region B1 resembling a "constant amplitude domain" showing a little or no variation of the amplitude over the range. A more generalized parametrical study of RSSs and other related nonlinear structures is beyond the scope of the present paper and will be communicated elsewhere.

ACKNOWLEDGMENTS

The authors would like to acknowledge the Director of Indian Institute of Geomagnetism for the facilities and encouragement for the completion of the work.

[1]M. Temerin, K. Cerny, W. Lotko, and F. S. Mozer, Phys. Rev. Lett. **48**, 1175–1179 (1982).
[2]H. Matsumoto, H. Kojima, T. Miyatake, Y. Omura, M. Okada, I. Nagano, and M. Tsutsu, Geophys. Res. Lett. **21**, 2915–2918, doi:10.1029/94GL01284 (1994).
[3]H. Matsumoto, H. Kojima, Y. Kasaba, T. Miyake, R. R. Anderson, and T. Mukai, Adv. Space Res. **20**, 683–693 (1997).
[4]S. D. Bale, P. J. Kellogg, D. E. Larson, R. P. Lin, K. Goetz, and R. P. Lepping, Geophys. Res. Lett. **25**, 2929–2932, doi:10.1029/98GL02111 (1998).
[5]C. A. Cattell, J. Dombeck, J. R. Wyganlt, M. K. Hudson, F. S. Mozer, M. A. Temerin, W. K. Peterson, C. A. Kletzings, C. T. Russell, and R. F. Pfaff, Geophys. Res. Lett. **26**, 425–428, doi:10.1029/1998GL900304 (1999).
[6]J. S. Pickett, J. D. Menietti, D. A. Gurnett, B. Tsurutani, P. M. Kintner, E. Klatt, and A. Balogh, Nonlinear Processes Geophys. **10**, 3–11 (2003).
[7]L. Muschietti, R. E. Ergun, I. Roth, and C. W. Carlson, Geophys. Res. Lett. **26**, 1093–1096, doi:10.1029/1999GL900207 (1999).
[8]N. Dubouloz, R. Pottelette, and M. Malingre, Geophys. Res. Lett. **18**, 155–158, doi:10.1029/90GL02677 (1991).
[9]S. S. Ghosh, J. S. Pickett, G. S. Lakhina, J. D. Winningham, B. Lavraud, and P. M. E. Decreau, J. Geophys. Res. **113**, A06218, doi:10.1029/2007JA012768 (2008).
[10]J. E. Wahlund, A. I. Eriksson, B. Holback, M. H. Boehm, J. Bonnell, P. M. Kintner, C. E. Seyler, J. H. Clemmons, L. Eliasson, D. J. Knudsen, P. Norqvists, and L. J. Zanetti, J. Geophys. Res. **103**, 4343–4375, doi:10.1029/97JA02008 (1998).
[11]J. Dombeck, C. Cattell, J. Crumle, W. K. Peterson, H. L. Coilin, and C. Kletzing, J. Geophys. Res. **106**, 19013–19021, doi:10.1029/2000JA000355 (2001).
[12]G. S. Lakhina, S. V. Singh, A. P. Kakad, F. Verheest, and R. Bharuthram, Nonlinear Processes Geophys. **15**, 903–913 (2008).
[13]P. H. Sakanaka, Phys. Fluids **15**, 304–310 (1972).
[14]R. B. White, B. D. Fried, and F. V. Coroniti, Phys. Fluids **15**, 1484–1490 (1972).
[15]H. Washimi and T. Taniuti, Phys. Rev. Lett. **17**, 996–998 (1966).
[16]M. Q. Tran and P. J. Hirt, Plasma Phys. **16**, 617–621 (1974).
[17]M. Q. Tran and Ch. Hollenstein, Phys. Rev. A **16**, 1284–1291 (1977).
[18]S. Bhattacharyya and R. K. Roychoudhury, Can. J. Phys. **66**, 467–470 (1988).
[19]S. S. Ghosh, K. K. Ghosh, and A. N. Sekar Iyengar, Phys. Plasmas **3**, 3939–3946 (1996).
[20]T. K. Baluku, M. A. Hellberg, and F. Verheest, Europhys. Lett. **91**, 15001 (2010).
[21]A. E. Dubinov and D. Yu. Kolotkov, Plasma Phys. Rep. **38**, 987–990 (2012).
[22]F. Verheest, M. A. Hellberg, and I. Kourakis, Phys. Plasmas **20**, 012302 (2013).
[23]F. Verheest, M. A. Hellberg, and I. Kourakis, Phys. Rev. E **87**, 043107 (2013).
[24]M. A. Hellberg, T. K. Baluku, F. Verheest, and I. Kourakis, J. Plasma Phys. **79**, 1039–1043 (2013).
[25]S. K. Maharaj, R. Bharuthram, S. V. Singh, and G. S. Lakhina, Phys. Plasmas **20**, 083705 (2013).
[26]F. Verheest, G. S. Lakhina, and M. A. Hellberg, Phys. Plasmas **21**, 062303 (2014).
[27]O. R. Rufai, R. Bharuthram, S. V. Singh, and G. S. Lakhina, Phys. Plasmas **21**, 082304 (2014).
[28]O. R. Rufai, R. Bharuthram, S. V. Singh, and G. S. Lakhina, Phys. Plasmas **22**, 102305 (2015).
[29]S. S. Ghosh and A. N. S. Iyengar, Phys. Plasmas **21**, 082104 (2014).
[30]S. S. Ghosh and A. N. S. Iyengar, J. Plasma Phys. **67**, 223–233 (2002).